IEEE Access
Multidisciplinary ⋮ Rapid Review ⋮ Open Access Journal

Received 5 May 2023, accepted 7 June 2023, date of publication 9 June 2023, date of current version 15 June 2023.

*Digital Object Identifier 10.1109/ACCESS.2023.3284753*

RESEARCH ARTICLE

# Fast Assessment of Rotor Barrier Dimensional Allowances in Synchronous Reluctance Machines

**CARLOS MADARIAGA[1], (Graduate Student Member, IEEE), CESAR GALLARDO[1,3], (Graduate Student Member, IEEE), JUAN A. TAPIA[1], (Senior Member, IEEE), WERNER JARA[2], (Member, IEEE), ANDRES ESCOBAR[2], AND MICHELE DEGANO[3], (Senior Member, IEEE)**

[1]Department of Electrical Engineering, University of Concepción, Concepción 4070386, Chile
[2]School of Electrical Engineering, Pontificia Universidad Católica de Valparaíso, Valparaíso 2362804, Chile
[3]Power Electronics, Machines and Control Group, University of Nottingham, NG7 2GT Nottingham, U.K.

Corresponding author: Carlos Madariaga (carlosmadariaga@udec.cl)

This work was supported in part by the Agencia Nacional de Investigación y Desarrollo (ANID), Chile, under Grant ANIDPFCHA/Doctorado Nacional/2020-21200350, Grant ANID-PFCHA/Doctorado Nacional/2020-21200527, Project FONDECYT REGULAR 1230670, and Project FONDEF ID21I10099.

**ABSTRACT** Tolerance analysis on synchronous reluctance machines (SynRM) is mandatory if accurate refinements of the rotor structure are adopted, a must for low-ripple applications However, the impact of manufacturing/dimensional tolerances or material degradation has been scarcely included in the design steps for SynRMs obeying complexity and time-requirement reasons. The paper provides an analysis of rotor barrier dimensional allowances in synchronous reluctance machines by utilizing a semi-analytical approach. This method is not only fast yet it also generates a substantial number of results that allows to evaluate the influence of dimensional deviations on the machine's performance. The proposed performance evaluation method is validated in four machines by direct finite element (FE) simulations, showing good agreement and low computational burden. Once validated, the method is applied to perform a brute-force search in a single-barrier 4-pole machine with different combinations of dimensional allowances, obtaining a significant reduction in computational time compared to traditional direct FE evaluation. The paper concludes with a description of the proposed methodology and its applicability to other SynRM designs. This opens the possibility of quickly analyzing tolerances in SynRMs and improving their performance by evaluating different dimensions and position of flux barriers.

**INDEX TERMS** Dimensional allowances, synchronous reluctance machine, torque ripple, average torque, fast performance evaluation method, full-range analysis.

## I. INTRODUCTION

Synchronous reluctance machines (SynRMs) have gained increasing attention in the past decade, especially in applications where enhanced efficiency and cost-effective power conversion is required [1]. When compared with the widely used induction motors (IMs), the absence of rotor windings in SynRM (as sketched in Fig. 1) leads to lower rotor losses and higher efficiency for the same frame size. Additionally, SynRM are proposed as a rare-earth magnet-free technology with a lower cost than permanent magnet (PM) machines [2], [3], [4]. Moreover, they are highly reliable, robust, and easy to maintain.

Nevertheless, they have two critical disadvantages, that have been discussed widely in literature, with an impact on their competitivity: the high torque ripple and the low power factor [5], [6], [7]. The performance of SynRM is strongly dependent on the rotor configuration and shape of the flux barriers [8]. Their dimension and position within the rotor, including the thickness and design of the iron bridges are main contributors of the torque ripple [9]. Accurate refinements of the rotor parameters are addressed in [10], [11],

The associate editor coordinating the review of this manuscript and approving it for publication was R. K. Saket.

This work is licensed under a Creative Commons Attribution-NonCommercial-NoDerivatives 4.0 License.
For more information, see https://creativecommons.org/licenses/by-nc-nd/4.0/

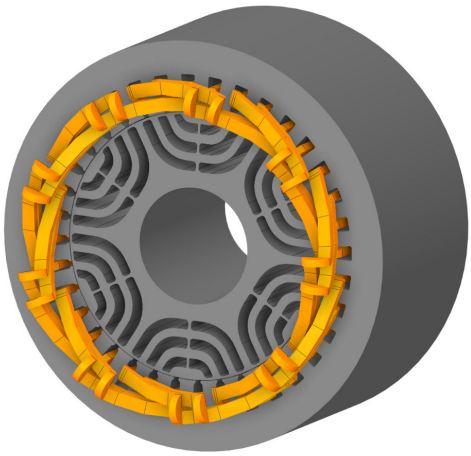

**FIGURE 1.** 3D sketch of a six-pole synchronous reluctance machine.

and [12] with the aim to reducing the torque ripple and improve the machine performance. In addition, algorithms for SynRM optimization can be found in [13], [14], and [15] aiming to tackle the torque ripple magnitude among other undesired effects. Notwithstanding, these analyses are based on designs with exact dimensions, and the impact of manufacturing/dimensional tolerances or material degradation has been scarcely included in the design steps for SynRM [9].

This issue is an aspect that has hardly been addressed for SynRM and it is a very critical aspect that can lead to significant differences between the expected performance (from the blueprint) and the built machine if the dimensional tolerances are not respected [9], [16], [17]: the expected torque ripple reduction may not be effectively obtained if dimensional deviations are present in the machine manufactured. In this regard, [16] provides a sensitivity analysis of torque ripple, and the authors stated that small geometry variations cause high torque ripple oscillations in several designs. This was further addressed in [9], where a robust design methodology is proposed. The selection of the robust design towards manufacturing tolerances among the best candidates is performed using statistical tools and worst-case analysis. The discussion emphasized that the optimal designs exhibit a strong deterioration of the torque ripple due to manufacturing tolerances. In [17], a topological optimization was used to consider the localized magnetic degradation on the lamination caused by punching process. This optimization method allowed to analyze small variations in the geometry of the machine and in [17], considerable differences in the torque ripple can be observed between the evaluated designs. Recently in [7], it was also disclosed that the high torque ripple of SynRM can be tackled by means of slight deviations in the rotor structure symmetry, which leads to significant performance variations. These studies raise a key design aspect: tolerance analysis on SynRM is mandatory if accurate refinements of the rotor structure are adopted, a must for low-ripple applications.

On the other hand, tolerance analysis cannot be conducted by means of the existing SynRM analytical models, obeying assumptions and accuracy reasons. Analytical models found in literature [18], [19], [20], [21], [22], [23], [24] do not consider the non-linearities of the machine and often limit its application to low-speed scenarios. Although these models are considerably helpful to derive preliminary design parameters, they are not compatible with the tolerance analysis requirements. In this regard, FE analysis is preferred [9], [16], [17], since it allows the incorporation of non-linearities to the machine materials, including the effect of saturation on the magnetizing current and the cross-saturation effect into the evaluations [24]. Nevertheless, a decisive drawback is faced when adopting FEA for conducting tolerance analyses: the computational burden is severe [9] when paired with optimization routines, and it has proven to scale with the pole count and the complexity of the rotor/stator structure [25]. In summary, a method that allows conducting an accurate yet fast dimensional allowance analysis on SynRM is lacking in literature.

The aim of this paper is thus to provide a fast yet accurate performance evaluation method for multi-barrier SynRMs including dimensional allowances and focusing on their electromagnetic torque generation. This opens the possibility of quickly analyzing tolerances in SynRMs and improving the performance of SynRMs by evaluating dimensions and position of flux barriers. In order to validate the method, four machines with different number of poles and flux barriers are evaluated by means of i) the proposed method and ii) direct FE simulations. Once the method is validated, a 4-pole machine with one flux barrier per pole is analyzed. A significant reduction in terms of computational time was obtained when compared with traditional direct FE evaluation, which enables conducting comprehensive tolerance analyses on SynRM with several deviated parameters.

The remaining part of this paper is organized as follows. In Section II the selection of the exemplary machines is described. The performance evaluation method is presented and validated for four SynRMs in Section III. An example of method applicability is given in Section IV where a full-range tolerance analysis is used. Conclusions are drawn at the end of the article.

## II. SELECTED MACHINES

With the aim of giving insight of the procedures behind the proposed performance evaluation method, four SynRM machines are considered and assessed in this work, as are presented in Fig. 2. Non-optimized SynRMs were considered in this work to obtain high ripple torque and better visualize the effect of rotor structure variations on the torque waveform.

Several geometrical parameters of the rotor structure affect to a greater or lesser amount the performance of the machine. The number of parameters increase exponentially as the number of flux barriers per pole and pole pairs increase and, therefore, there are several design guidelines established in the literature to choose the number of flux barriers and poles.

SynRM is designed to maximize d-axis inductance and minimize q-axis inductance as this ensures that the machine's

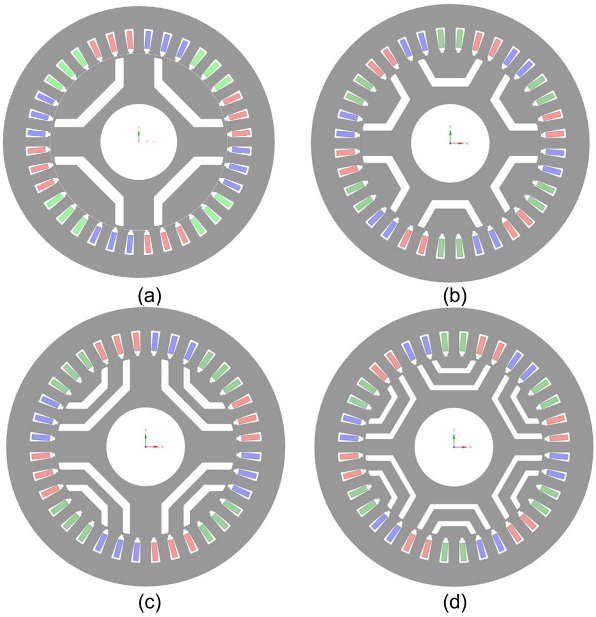


**FIGURE 2.** 2D schematics of SynRMs: (a) four pole with one barrier; (b) four pole with two barrier; (c) six pole with one barrier; (d) six pole with two barrier. Three-phase stator windings are highlighted in red, green, and blue.

**TABLE 1.** Main data of selected SynRM.

| Parameter | Symbol | Value |
|---|---|---|
| Stator outer diameter | $D_{so}$ | 245 mm |
| Stator inner diameter | $D_{si}$ | 161.4 mm |
| Rotor outer diameter | $D_{ro}$ | 160.4 mm |
| Rotor inner diameter | $D_{ri}$ | 70 mm |
| Tooth height | $h_t$ | 22.8 mm |
| Tooth width | $b_t$ | 9 mm |
| Air-gap length | g | 0.5 mm |
| Stack length | $l_{st}$ | 120 mm |
| Turns per slot | $N_s$ | 20 |
| Number of slots | $Q_s$ | 36 |
| Speed | n | 3000 rpm |
| Current Density | J | 10 A/mm$^2$ |
| Current angle | $\alpha_i^e$ | 60°electric |

saliency ratio is large enough for the machine's performance ratings to meet the standards. On the one hand, and in order to obtain a good saliency ratio, a small number of pole pairs is preferred, and the technical literature recommends adopting two or three pole pairs [26]. On the other hand, the optimum number of flux barriers is defined according to the number of stator slots. For the case of a 36-slot machine, some authors do not encourage to adopt more than three flux barriers. A greater number of barriers could affect the rotor mechanical integrity or increase the design process complexity [11], [27].

Therefore, in this paper exemplary machines with two and three pole pairs are considered, and each pole can adopt one or two barriers, summing up to a total of four machines. The common data for all machines are presented in Table 1.

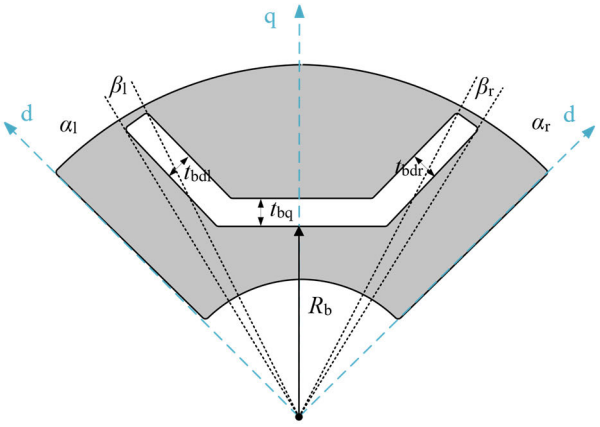


**FIGURE 3.** Schematics of the rotor structure for a 1-barrier configuration.

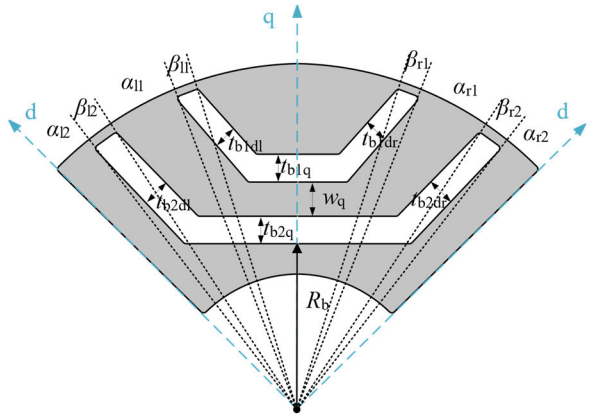


**FIGURE 4.** Schematics of the rotor structure for a 2-barrier configuration.

**TABLE 2.** Main data of 1-barrier rotor.

| | | 4-pole | 6-pole |
|---|---|---|---|
| Parameter | Symbol | Value | Value |
| Flux barrier position (right) | $\alpha_r$ | 8° | 8° |
| Flux barrier position (left) | $\alpha_l$ | 8° | 8° |
| Flux barrier opening (right) | $\beta_r$ | 5° | 5° |
| Flux barrier opening (left) | $\beta_l$ | 5° | 5° |
| Flux barrier width q-axis | $t_{b_q}$ | 10 mm | 8 mm |
| Flux barrier width d-axis (right) | $t_{b_{dr}}$ | 5° | 5° |
| Flux barrier width d-axis (left) | $t_{b_{dl}}$ | 5° | 5° |
| Inner barrier radius | $R_b$ | 45 mm | 50 mm |
| Insulation ratio | $k_{air}$ | 0.11 | 0.08 |

Parameters considered for the proposed method

The rotor data are shown in Tables 2 and 3 for the machines with one and two barriers respectively. For visualization means, Fig. 3 and Fig. 4 show the schematic of the rotor parameters for the selected one-barrier and two-barrier machines, respectively.

In [16] the impact of geometrical parameters on torque is analyzed, and the sensitivity of an optimal solution to geom-

**TABLE 3.** Main data of 2-barrier rotor.

| Parameter | Symbol | 4-pole Value | 6-pole Value |
|---|---|---|---|
| Flux barrier (1) position (right) | $\alpha_{r1}$ | 10° | 6° |
| Flux barrier (1) position (left) | $\alpha_{l1}$ | 10° | 6° |
| Flux barrier (2) position (right) | $\alpha_{r2}$ | 10° | 5° |
| Flux barrier (2) position (left) | $\alpha_{l2}$ | 10° | 5° |
| Flux barrier (1) opening (right) | $\beta_{r1}$ | 5° | 4° |
| Flux barrier (1) opening (left) | $\beta_{l1}$ | 5° | 4° |
| Flux barrier (2) opening (right) | $\beta_{r2}$ | 5° | 4° |
| Flux barrier (2) opening (left) | $\beta_{l2}$ | 5° | 4° |
| Flux barrier (1) width q-axis | $t_{b_{q1}}$ | 8 mm | 5 mm |
| Flux barrier (2) width q-axis | $t_{b_{q2}}$ | 8 mm | 5mm |
| Flux barrier (1) width d-axis (right) | $t_{b_{dr1}}$ | 5° | 4° |
| Flux barrier (1) width d-axis (left) | $t_{b_{dl1}}$ | 5° | 4° |
| Flux barrier (2) width d-axis (right) | $t_{b_{dr2}}$ | 5° | 4° |
| Flux barrier (2) width d-axis (left) | $t_{b_{dl2}}$ | 5° | 4° |
| Width between barrier 1-2 | $w_q$ | 7 mm | 10 mm |
| Inner barrier radius | $R_b$ | 60 mm | 65 mm |
| Insulation ratio | $k_{air}$ | 0.17 | 0.11 |

Parameters considered for the proposed method

etry variation is pointed out. It is observed that the variation of the third flux-barrier angle can significantly affect the torque ripple. A sensitivity analysis performed in [7] shows similar results to those presented in [16]. It is also observed that incorporating asymmetric barriers in the rotor allows to reduce the influence of the barrier angle to provide higher degrees of freedom. Therefore, in this work the position of the barriers is varied since it has proven to develop a significant impact on the torque ripple.

## III. PERFORMANCE EVALUATION METHOD

In this section, the proposed approach to predict the impact of dimensional deviations of rotor barriers on the electromagnetic torque is described and validated. This methodology is inspired by the one developed by the authors in [25] and [28].

### A. ASSUMPTIONS/CONSIDERATIONS

In a real manufacturing process, multiple structural units can exhibit failures (and a combination of them) and penalize its electromagnetic performance. For a single parameter subject to a discrete tolerance analysis, if $F$ failures are considered in addition to the flawless condition, a total of $F+1$ possible combinations can be assessed. In Fig. 5, the representation of possible failures with $F = 2$ is presented. In this case, the parameter $\alpha_r$ can adopt three values ($i = 1, 2$ and 3) depending on the upper limit of the allowance range ($\Delta$):

- $\alpha_{r1} = -\Delta$
- $\alpha_{r2} = 0$
- $\alpha_{r3} = \Delta$

If $F$ is higher, then more values of $\alpha_r$ must be evaluated within the range $[-\Delta, \Delta]$.

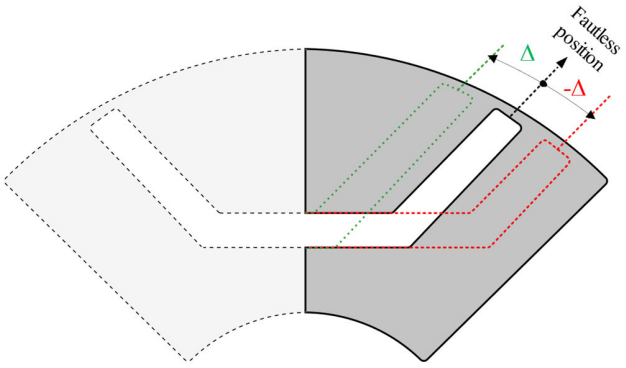


**FIGURE 5.** Schematics of possible failures with $F = 2$ on the right side of a barrier of a single pole.

For the topology under analysis, which has 2p poles and b barriers, the number of possible combinations which require to be evaluated (combinations of $\alpha_{ri}$ and $\alpha_{li}$, with $i = 1, 2, \ldots, F+1$) are

$$Q_{\text{eval}} = (F+1)^{4p \cdot b}. \tag{1}$$

This means that, with the aim to assess the combinations of $\alpha_{ri}$ and $\alpha_{li}$ on a 4-pole 1-barrier SynRM resulting from $F = 6$, a total of ~5.7 million designs should be evaluated. This is unfeasible only by means of FE simulations.

Therefore, in order to accelerate the analysis of the effect of all possible combinations of deviated barriers over SynRM, a method based on the superposition technique is used [11], [25], [26], [27], [28]. Its main assumptions and considerations are summarized below:

The dimensional range of each parameter is discretized depending on the value of $F$.

- Poles are considered as relatively independent structural units, in terms of their electromagnetic response.
- The method can consider saturation since it relies on the results from direct FE evaluation.

### B. EXPRESSIONS

The proposed method aims to reconstruct the torque waveform considering the error contribution of all the barriers on the machine, as explained in the sketch shown in Fig. 6.

When the $m$-th barrier of a certain pole (reference pole) is displaced in a machine called $X$, there will be a difference between the developed torque of the machine $X$ and the flawless design, called error, which depends on the magnitude of the displacement given by $i$. Therefore, the error generated by displacement of the left side of the $m$-th barrier can be represented as:

$$\xi_{lmi}(\theta_r) = \mathrm{T}_{lmi}(\theta_r) - \mathrm{T}_f(\theta_r), \tag{2}$$

where $\mathrm{T}_f$ is the torque waveform of the flawless machine, and $\mathrm{T}_{lmi}$ is the torque waveform of a machine which left side of the m-th barrier is affected by a deviation magnitude (related to $i$). In turn, the error generated by displacements of the right

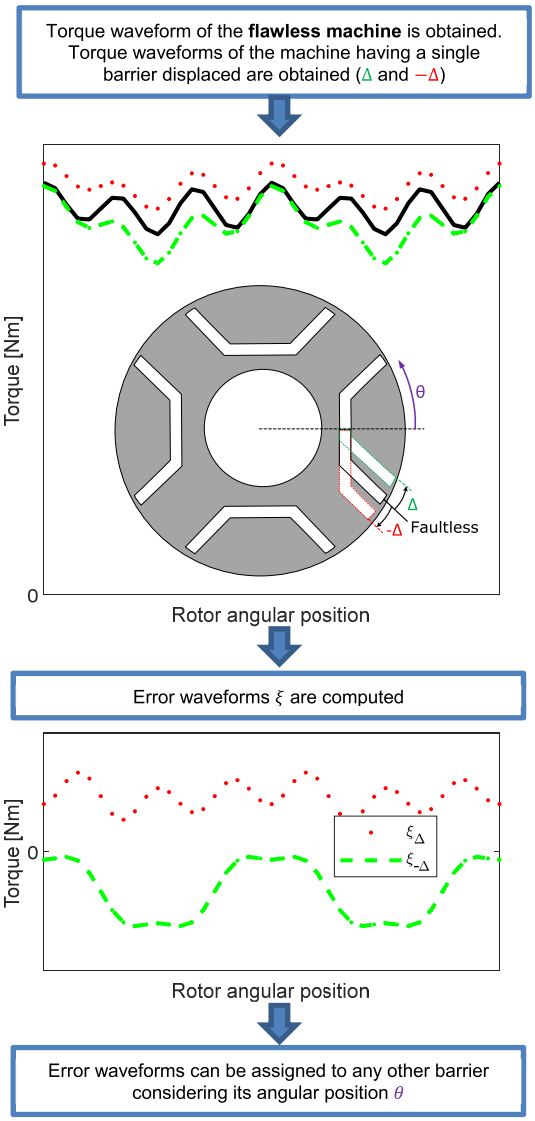


**FIGURE 6.** Sketch of the proposed methodology. Error waveforms are obtained to reconstruct the torque of faulty machines.

side of the m-th barrier is:

$$\xi_{rmi}(\theta_r) = \mathrm{T}_{rmi}(\theta_r) - \mathrm{T}_f(\theta_r), \tag{3}$$

where $\mathrm{T}_{rmi}$ is the torque waveform of a machine which right side of the m-th barrier is affected by a deviation magnitude (related to $i$). Both $\xi_{lmi}(\theta_r)$ and $\xi_{rmi}(\theta_r)$ for $m = 1, 2, \ldots, b$ and $i = 1, 2, \ldots, F+1$ can be obtained from FE simulations considering deviations on a single pole of the machine, called reference pole. Therefore, the torque of the machine considering all possible deviations on the reference pole of the machine is given by:

$$\mathrm{T}_{\mathrm{RP}}(\theta_r) = \mathrm{T}_f(\theta_r) + \sum_{m=1}^{b} \{\xi_{lmi}(\theta_r) + \xi_{rmi}(\theta_r)\} \tag{4}$$

If the barriers of the other poles are to be evaluated considering misplacement, then a superposition approach can be applied. Displacing the $m$-th barrier of a certain pole has the same error waveform as displacing the $m$-th barrier of the reference pole but shifted. This is a crucial aspect of the methodology: the errors of a pole other than the reference can be obtained from the reference ones, considering a mechanical angular shift ($\gamma$) that can be calculated as:

$$\gamma_n = \frac{360}{2p} n \tag{5}$$

where n is the distance in number of poles between the pole that is desired to be assessed and the reference pole (for which the error waveforms were computed by means of FEA).

Thus, the torque of a machine with any combination of displacements on its barriers can be computed as:

$$\mathrm{T}_{\mathrm{final}}(\theta_r) = \mathrm{T}_f(\theta_r) + \sum_{n=1}^{2p-1} \sum_{m=1}^{b} \{\xi_{lmi}(\theta_r - \gamma_n) + \xi_{rmi}(\theta_r - \gamma_n)\}. \tag{6}$$

where $\mathrm{T}_f(\theta_r)$ is the torque waveform of the faultless machine, $\mathrm{T}_{lmi}(\theta_r)$ is the torque waveform of the machine with a deviation on the position of the left side of the m-th barrier of any pole; and $\mathrm{T}_{rmi}(\theta_r)$ is the torque waveform of the machine with a deviation on the position of the right side of the m-th barrier of any pole. The parameter i allows to select different displacements, as described in Section III-A. The flowchart for implementing the proposed method is presented in Fig. 7.

### C. VALIDATION

In order to validate the proposed torque reconstruction method, the four machines presented in Fig. 2 are evaluated with different displacement values ($\alpha_{ri}$). This validation consists of comparing the outcome of:

- The proposed method, which requires a few simulation runs to obtain input torque waveforms. These waveforms are used to estimate the torque of several machines with deviated dimensional parameters.
- Direct FE evaluation of machines with deviated dimensional parameters.

FE simulation was carried out using ANSYS Electronic Desktop software package for a rotor speed of 3000 rpm and an RMS current density of 11.8 A/mm$^2$. The current angle was fixed at 60 electrical degrees and the magnetic steel chosen was M350-50A. For both cases, a high-density mesh was considered for the airgap, bridge and barrier zones to obtain an accurate input for the proposed semi-analytical method and a fair comparison between results. In Fig. 8, the used FE model and the obtained flux density distribution for the flawless case are presented. A maximum value of ∼2.3 T was obtained around the bridges and ∼1.8 T in the teeth and stator-yoke areas. In this sense, mild saturation is considered in this paper to demonstrate the applicability of the proposed method.

Exaggerated displacements on the left side and the right side of the barriers of the machine were considered (see Fig. 5). This, in order to obtain significant torque variations

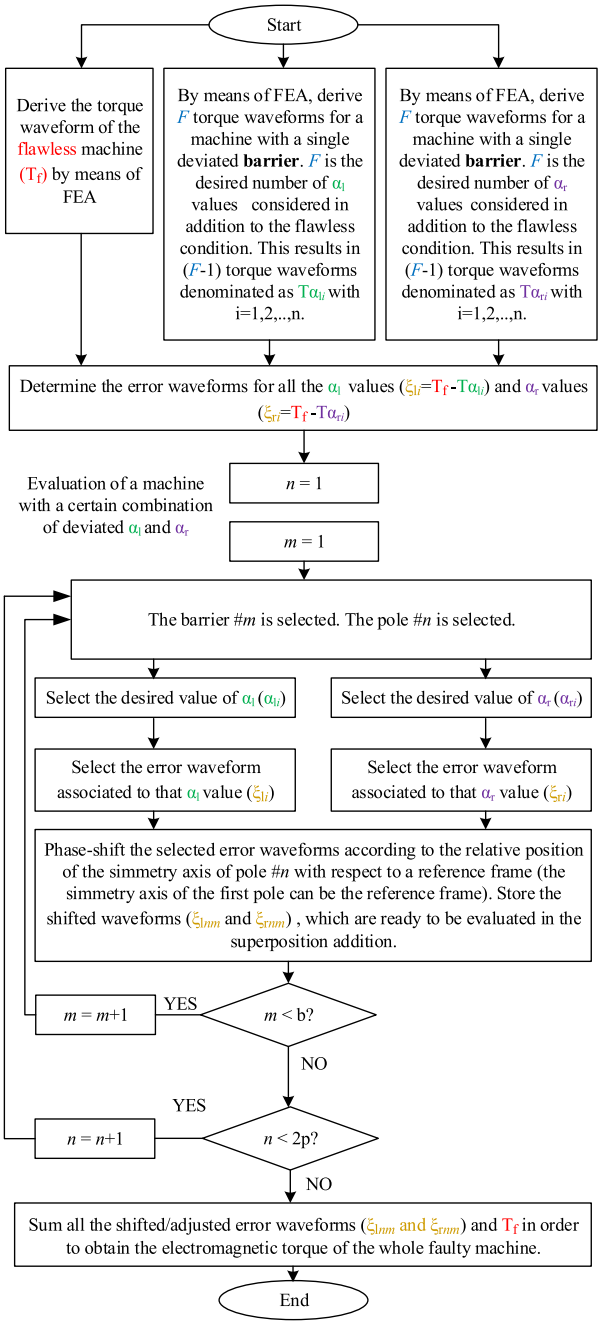


**FIGURE 7.** Flowchart of the proposed methodology to estimate torque waveforms from a few FE simulation runs.

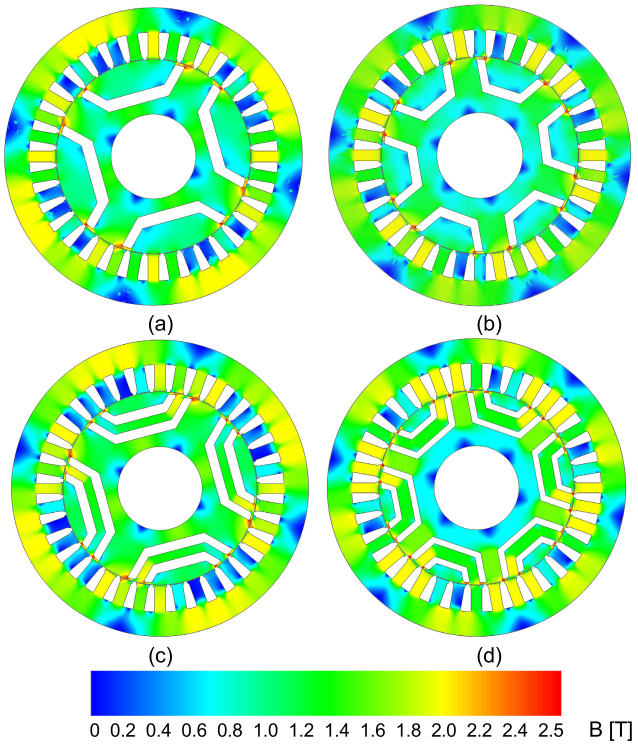


**FIGURE 8.** Flux density distribution of the selected machines without dimensional deviations: (a) four pole with one barrier; (b) six pole with one barrier; (c) four pole with two barrier; (d) six pole with two barrier.

with respect to the flawless machine and disclose the differences between the proposed method and direct FE evaluation.

The comparison of the rated torque between FEA and the proposed method for the validation scenarios is presented in Fig. 9. Table 5 in Appendix summarize the data of the validation scenarios considered, including the dimensional deviation magnitude and the barriers and poles affected by dimensional deviations. These scenarios were selected in order to consider i) severe dimensional deviations acting on a single barrier that is different to that evaluated in the first steps of the methodology (See Fig. 6); ii) dimensional deviations acting on both sides of barriers; iii) dimensional deviations acting on different sides of several barriers simultaneously. From Fig. 8, it can be observed that in all cases, the results provided by the different methods show good agreement, even when there are significant waveform changes between scenarios and mild saturation is taken into account.

Additionally, a second validation of 100 machine designs with randomly generated dimensional deviations was carried out with accurate results. Comparing the torque waveforms estimated by the proposed method with those obtained by direct FE evaluation provided a mean average error lower than 6%. In order to replicate this accuracy when implementing the proposed method, a mesh with high quality elements and a minimum number of samples of the simulations runs subject to the Nyquist theorem is recommended. Likewise, if reducing the simulation time is required, it is possible to simulate only one electrical period to obtain the basal simulation results. In turn, there are no restrictions that must be followed regarding material selection to obtain accurate estimations.

## IV. BRUTE-FORCE TOLERANCE ANALYSIS: AN EXAMPLE OF APPLICABILITY

SynRMs have a complex rotor structure with many geometrical parameters that can affect its performance. As a result, there are many possible machine combinations that need to

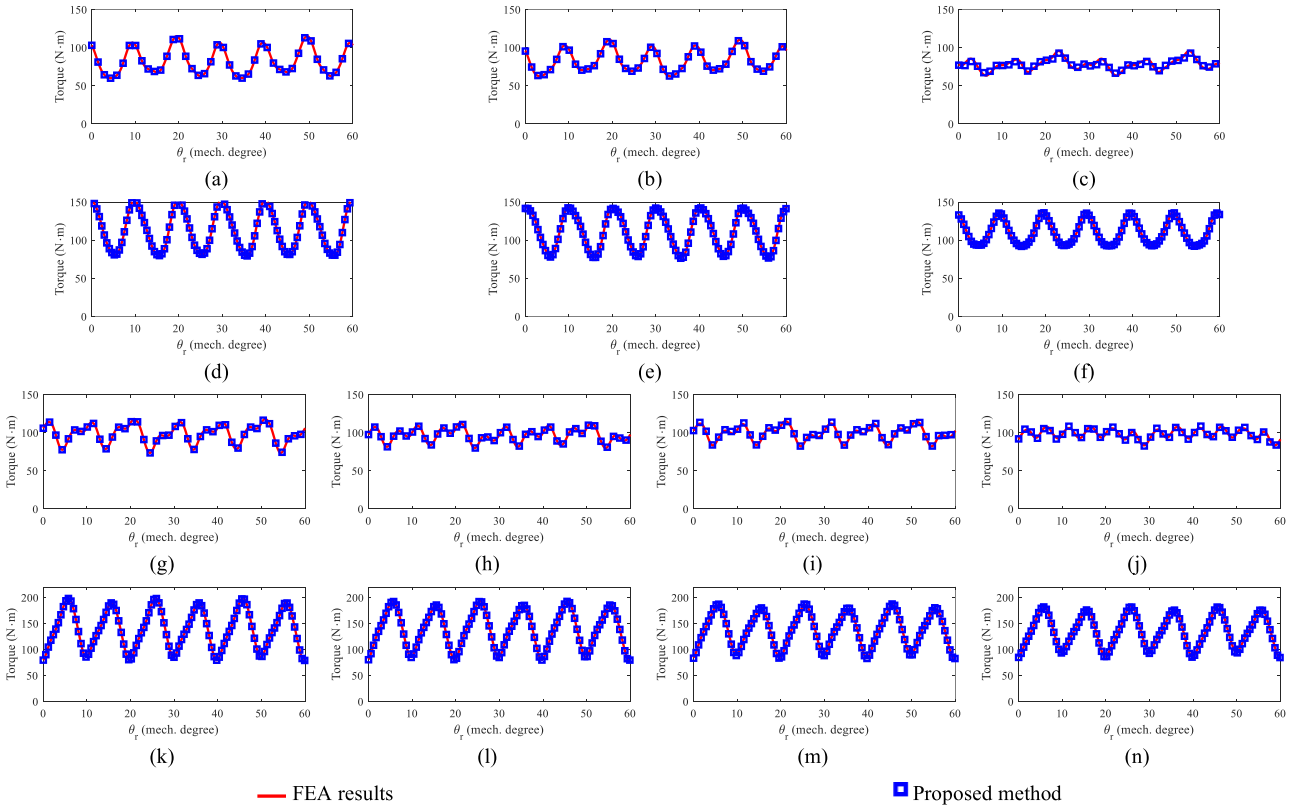


**FIGURE 9.** Comparison of the rated torque between FEA and the proposed method, considering (a), (b), (c) 4P1B machine (d), (e), (f) 6P1B machine; (g), (h), (i), (j) 4P2B machine, and (k), (l), (m), (n) 6P2B machine. Specifications of these scenarios can be found in Annex.

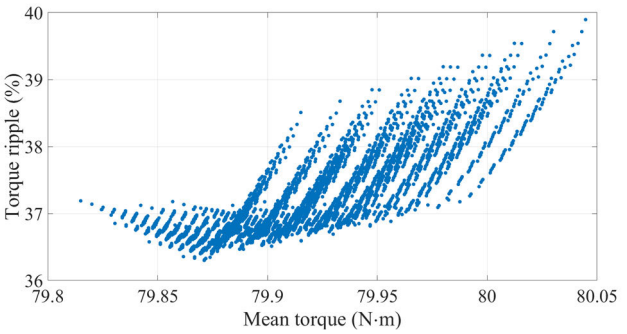


**FIGURE 10.** Average torque and ripple torque obtained for a SynRM with 36 slots, 4 poles and one barrier per pole when manufacturing tolerances are present. The values are achieved for one and two times the typical manufacturing tolerance of a laser cutter machine (±0.1mm), and using the method described in Fig. 6 and Fig. 7.

**TABLE 4.** Best and worst values of average torque and ripple torque obtained for a SynRM with 36 slots, 4 poles and one barrier per pole when manufacturing tolerances are present.

| Case | Torque ripple | Mean torque |
|---|---|---|
| Best ripple | 36.3% | 79.9 Nm |
| Worst ripple | 39.9 % | 80.1 Nm |
| Best mean torque | 39.9 % | 80.1 Nm |
| Worst mean torque | 37.2% | 79.8 Nm |

be analyzed to take into account manufacturing tolerances, as described in (1).

A 4-pole machine with one flux barrier per pole is considered as an example. Typical manufacturing tolerances can be used to determine the possible values that each dimension of the machine can adopt as suggested in [25]. Let us consider five possible values of the rotor barrier position, then these can be:

- The originally conceived value (flawless).
- The original value deviated in the typical manufacturing tolerance (two possibilities, ±0.1 mm for laser cutting)
- Twice the standard manufacturing tolerance for a laser cutting machine (Two options: ±0.2mm),

As a result, and according to (1), it is necessary to analyze approximately ∼390,000 designs in order to perform an accurate analysis. In this section, the proposed method is used to perform a full-range tolerance analysis of 4-pole SynRM, considering the five options indicated above. The average torque and torque ripple values resulting from this analysis are shown in Fig. 10.

Analyzing these ∼390,000 designs took a total time of 100 hours considering the 9 FEA simulations using the commercial package ANSYS Electronic Desktop and considering

**TABLE 5.** All cases considered to assess the proposed method (using exaggerated tolerance values).

| | | $b_{11l}$ | $b_{11r}$ | $b_{21l}$ | $b_{21r}$ | $b_{31l}$ | $b_{31r}$ | $b_{41l}$ | $b_{41r}$ | $b_{51l}$ | $b_{51r}$ | $b_{61l}$ | $b_{61r}$ |
|---|---|---|---|---|---|---|---|---|---|---|---|---|---|
| 4P1B | SC1 | 0 | 0 | 0 | 0 | 0 | +4 | 0 | 0 | - | - | - | - |
| | SC2 | 0 | 0 | -4 | +4 | 0 | 0 | 0 | 0 | - | - | - | - |
| | SC3 | 0 | 0 | 0 | +4 | +4 | -4 | +4 | -4 | - | - | - | - |
| 6P1B | SC1 | 0 | 0 | 0 | 0 | -4 | 0 | 0 | 0 | 0 | 0 | 0 | 0 |
| | SC2 | 0 | 0 | 0 | 0 | 0 | 0 | 0 | 0 | +4 | -4 | 0 | 0 |
| | SC3 | 0 | 0 | -4 | +4 | -4 | 0 | 0 | 0 | 0 | 0 | 0 | +4 |
| 4P2B | SC1 | $b_{11l}$ | $b_{11r}$ | $b_{21l}$ | $b_{21r}$ | $b_{31l}$ | $b_{31r}$ | $b_{41l}$ | $b_{41r}$ | $b_{51l}$ | $b_{51r}$ | $b_{61l}$ | $b_{61r}$ |
| | | 0 | 0 | 0 | 0 | -4 | 0 | 0 | 0 | - | - | - | - |
| | | $b_{12l}$ | $b_{12r}$ | $b_{22l}$ | $b_{22r}$ | $b_{32l}$ | $b_{32r}$ | $b_{42l}$ | $b_{42r}$ | $b_{52l}$ | $b_{52r}$ | $b_{62l}$ | $b_{62r}$ |
| | | 0 | 0 | 0 | 0 | 0 | 0 | 0 | 0 | - | - | - | - |
| | SC2 | $b_{11l}$ | $b_{11r}$ | $b_{21l}$ | $b_{21r}$ | $b_{31l}$ | $b_{31r}$ | $b_{41l}$ | $b_{41r}$ | $b_{51l}$ | $b_{51r}$ | $b_{61l}$ | $b_{61r}$ |
| | | 0 | 0 | 0 | 0 | 0 | 0 | +4 | 0 | - | - | - | - |
| | | $b_{12l}$ | $b_{12r}$ | $b_{22l}$ | $b_{22r}$ | $b_{32l}$ | $b_{32r}$ | $b_{42l}$ | $b_{42r}$ | $b_{52l}$ | $b_{52r}$ | $b_{62l}$ | $b_{62r}$ |
| | | 0 | 0 | 0 | 0 | 0 | 0 | 0 | +4 | - | - | - | - |
| | SC3 | $b_{11l}$ | $b_{11r}$ | $b_{21l}$ | $b_{21r}$ | $b_{31l}$ | $b_{31r}$ | $b_{41l}$ | $b_{41r}$ | $b_{51l}$ | $b_{51r}$ | $b_{61l}$ | $b_{61r}$ |
| | | 0 | 0 | -4 | 0 | 0 | 0 | 0 | 0 | - | - | - | - |
| | | $b_{12l}$ | $b_{12r}$ | $b_{22l}$ | $b_{22r}$ | $b_{32l}$ | $b_{32r}$ | $b_{42l}$ | $b_{42r}$ | $b_{52l}$ | $b_{52r}$ | $b_{62l}$ | $b_{62r}$ |
| | | 0 | 0 | -4 | -4 | 0 | 0 | 0 | 0 | - | - | - | - |
| | SC4 | $b_{11l}$ | $b_{11r}$ | $b_{21l}$ | $b_{21r}$ | $b_{31l}$ | $b_{31r}$ | $b_{41l}$ | $b_{41r}$ | $b_{51l}$ | $b_{51r}$ | $b_{61l}$ | $b_{61r}$ |
| | | 0 | 0 | 0 | 0 | 0 | -4 | 0 | -4 | - | - | - | - |
| | | $b_{12l}$ | $b_{12r}$ | $b_{22l}$ | $b_{22r}$ | $b_{32l}$ | $b_{32r}$ | $b_{42l}$ | $b_{42r}$ | $b_{52l}$ | $b_{52r}$ | $b_{62l}$ | $b_{62r}$ |
| | | 0 | 0 | 0 | -4 | +4 | +4 | 0 | 0 | - | - | - | - |
| 6P2B | SC1 | $b_{11l}$ | $b_{11r}$ | $b_{21l}$ | $b_{21r}$ | $b_{31l}$ | $b_{31r}$ | $b_{41l}$ | $b_{41r}$ | $b_{51l}$ | $b_{51r}$ | $b_{61l}$ | $b_{61r}$ |
| | | 0 | 0 | 0 | 0 | 0 | -3 | 0 | 0 | 0 | 0 | 0 | 0 |
| | | $b_{12l}$ | $b_{12r}$ | $b_{22l}$ | $b_{22r}$ | $b_{32l}$ | $b_{32r}$ | $b_{42l}$ | $b_{42r}$ | $b_{52l}$ | $b_{52r}$ | $b_{62l}$ | $b_{62r}$ |
| | | 0 | 0 | 0 | 0 | 0 | 0 | 0 | 0 | 0 | 0 | 0 | 0 |
| | SC2 | $b_{11l}$ | $b_{11r}$ | $b_{21l}$ | $b_{21r}$ | $b_{31l}$ | $b_{31r}$ | $b_{41l}$ | $b_{41r}$ | $b_{51l}$ | $b_{51r}$ | $b_{61l}$ | $b_{61r}$ |
| | | 0 | 0 | 0 | 0 | 0 | 0 | 0 | +3 | 0 | 0 | 0 | 0 |
| | | $b_{12l}$ | $b_{12r}$ | $b_{22l}$ | $b_{22r}$ | $b_{32l}$ | $b_{32r}$ | $b_{42l}$ | $b_{42r}$ | $b_{52l}$ | $b_{52r}$ | $b_{62l}$ | $b_{62r}$ |
| | | 0 | 0 | 0 | 0 | 0 | 0 | -3 | 0 | 0 | 0 | 0 | 0 |
| | SC3 | $b_{11l}$ | $b_{11r}$ | $b_{21l}$ | $b_{21r}$ | $b_{31l}$ | $b_{31r}$ | $b_{41l}$ | $b_{41r}$ | $b_{51l}$ | $b_{51r}$ | $b_{61l}$ | $b_{61r}$ |
| | | 0 | 0 | 0 | 0 | 0 | 0 | 0 | 0 | 0 | +3 | 0 | 0 |
| | | $b_{12l}$ | $b_{12r}$ | $b_{22l}$ | $b_{22r}$ | $b_{32l}$ | $b_{32r}$ | $b_{42l}$ | $b_{42r}$ | $b_{52l}$ | $b_{52r}$ | $b_{62l}$ | $b_{62r}$ |
| | | 0 | 0 | 0 | 0 | 0 | 0 | 0 | 0 | -3 | +3 | 0 | 0 |
| | SC4 | $b_{11l}$ | $b_{11r}$ | $b_{21l}$ | $b_{21r}$ | $b_{31l}$ | $b_{31r}$ | $b_{41l}$ | $b_{41r}$ | $b_{51l}$ | $b_{51r}$ | $b_{61l}$ | $b_{61r}$ |
| | | 0 | 0 | +3 | -3 | 0 | 0 | 0 | 0 | 0 | 0 | +3 | 0 |
| | | $b_{12l}$ | $b_{12r}$ | $b_{22l}$ | $b_{22r}$ | $b_{32l}$ | $b_{32r}$ | $b_{42l}$ | $b_{42r}$ | $b_{52l}$ | $b_{52r}$ | $b_{62l}$ | $b_{62r}$ |
| | | 0 | 0 | -3 | 0 | 0 | 0 | 0 | 0 | 0 | 0 | +3 | 0 |

the time MATLAB took to evaluate the method with the simulation results as inputs. A fine mesh has been applied with ∼705,000 nodes, and the torque ripple waveform have been determined considering a full revolution and a total of about 20,000 samples. To put that into perspective, the same study using only FEA simulations would take about 122,000 hours in the same computer (equivalent to 14 years) when a course mesh is used and only one period of the torque ripple is simulated. Therefore, the described method allows us to analyze all possible combinations in 0.1% of the time it would take when only FEA simulations are used.

Table 4 presents the average torque and ripple torque values for the best and worst case of all analyzed designs. It is possible to appreciate that the average torque does not present considerable variations, which is to be expected because in a SynRM the position of the flux barrier mostly affects the ripple torque value. The variation on the torque ripple between the best and the worst case is around a 9%. This result is mostly due to the different combinations of the flux barrier's positions that create asymmetrical designs and cancel combination of harmonics in electromagnetic torque [7].

The electromagnetic torque waveform for the best and worst value of torque ripple is presented in Fig. 11. Both waveforms are quite similar, with slight changes appearing due to the variation of the relative position between the rotor flux barriers and the stator teeth in each design. In this sense, the ripple torque of this particular machine design can be considered as insensitive to the barrier angular displacement tolerances. Moreover, it can be observed that the presence of manufacturing tolerances does not cause new harmonics

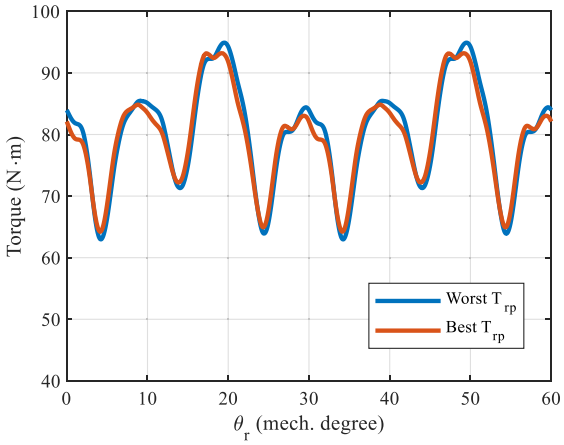


**FIGURE 11. Electromagnetic torque waveform considering two torque ripple periods for the best and worst cases obtained for a SynRM with 36 slots, 4 poles and one barrier per pole when manufacturing tolerances are present.**

components to appear in the electromagnetic torque of the machine.

## V. CONCLUSION

This paper presented a detailed analysis of rotor barrier dimensional allowances for SynRMs, utilizing a semi-analytical procedure usually adopted for static analysis in permanent magnet machines. The aim of the assessment is estimating the torque ripple of the machine, which strongly relies on rotor geometry parameters. The proposed method proved to be faster than conventional direct FE evaluation and was able to generate a significant number of results to deeply assess the impact of barrier dimensional deviations on the SynRM performance. The validation was carried out by means of direct FEA for a wide range of cases, and the comparative results are all in good agreement.

Results showed a significant computation time reduction, of around 99.9% with respect to directly evaluating rotor barrier allowance effects on the torque ripple. This enables performing thorough tolerance analysis on the rotor geometry, as well as evaluating asymmetric designs. The method was also applied to a specific case study to show its applicability as a brute-force search tool for the assessment of torque ripple in slightly variated scenarios of a final SynRM design. The proposed method aimed to be general and configure as a useful tool to SynRM designers that can be successfully applied for different number of poles and flux barriers. Hereafter, it is possible to apply the method to calculate other performance indices that can obtained from the airgap flux density or electromagnetic torque. In consequence, it may be possible to use the method to calculate radial and tangential forces on the rotor, losses, and efficiency. Future research is yet to be done to cover this topic.

## APPENDIX

Table 5 presents the dimensional parameters of the machines used for validation purposes. These parameters are grouped considering evaluation scenarios, selected in order to consider:

i. Severe dimensional deviations acting on a single barrier that is different to that evaluated in the first steps of the methodology (see Fig. 6 and Fig. 7). This is the case of SC1 for the four selected machines.
ii. Dimensional deviations acting on both sides of barriers. This is the case of SC2 for the four selected machines.
iii. Dimensional deviations acting on different sides of several barriers simultaneously. This is the case of SC3 and SC4.

## REFERENCES

[1] O. Korman, M. D. Nardo, M. Degano, and C. Gerada, "A novel flux barrier parametrization for synchronous reluctance machines," *IEEE Trans. Energy Convers.*, vol. 37, no. 1, pp. 675–684, Mar. 2022.
[2] H. Kim, Y. Park, S. Oh, G. Jeong, U. Seo, S. Won, and J. Lee, "Study on analysis and design of line-start synchronous reluctance motor considering rotor slot opening and bridges," *IEEE Trans. Magn.*, vol. 58, no. 2, pp. 1–6, Feb. 2022.
[3] J. M. Park, S. I. Kim, J. P. Hong, and J. H. Lee, "Rotor design on torque ripple reduction for a synchronous reluctance motor with concentrated winding using response surface methodology," *IEEE Trans. Magn.*, vol. 42, no. 10, pp. 3479–3481, Oct. 2006.
[4] J.-B. Im, W. Kim, K. Kim, C.-S. Jin, J.-H. Choi, and J. Lee, "Inductance calculation method of synchronous reluctance motor including iron loss and cross magnetic saturation," *IEEE Trans. Magn.*, vol. 45, no. 6, pp. 2803–2806, Jun. 2009.
[5] J. K. Kostko, "Polyphase reaction synchronous motors," *J. Amer. Inst. Electr. Eng.*, vol. 42, no. 11, pp. 1162–1168, Nov. 1923.
[6] A. Fratta, G. P. Toglia, A. Vagati, and F. Villata, "Ripple evaluation of high-performance synchronous reluctance machines," *IEEE Ind. Appl. Mag.*, vol. 1, no. 4, pp. 14–22, Aug. 1995.
[7] C. Gallardo, J. A. Tapia, M. Degano, H. Mahmoud, and A. E. Hoffer, "Rotor asymmetry impact on synchronous reluctance machines performance," in *Proc. Int. Conf. Electr. Mach. (ICEM)*, 2022, pp. 848–854.
[8] S. T. Boroujeni, M. Haghparast, and N. Bianchi, "Optimization of flux barriers of line-start synchronous reluctance motors for transient- and steady-state operation," *Electric Power Compon. Syst.*, vol. 43, no. 5, pp. 594–606, Mar. 2015.
[9] A. Credo, G. Fabri, M. Villani, and M. Popescu, "A robust design methodology for synchronous reluctance motors," *IEEE Trans. Energy Convers.*, vol. 35, no. 4, pp. 2095–2105, Dec. 2020.
[10] A. Credo, G. Fabri, M. Villani, and M. Popescu, "High speed synchronous reluctance motors for electric vehicles: A focus on rotor mechanical design," in *Proc. IEEE Int. Electric Mach. Drives Conf. (IEMDC)*, May 2019, pp. 165–171.
[11] M. N. F. Ibrahim, P. Sergeant, and E. Rashad, "Simple design approach for low torque ripple and high output torque synchronous reluctance motors," *Energies*, vol. 9, no. 11, p. 942, 2016.
[12] C. Liu, K. Wang, S. Wang, Y. Wang, and J. Zhu, "Torque ripple reduction of synchronous reluctance machine by using asymmetrical barriers and hybrid magnetic core," *CES Trans. Electr. Mach. Syst.*, vol. 5, no. 1, pp. 13–20, Mar. 2021.
[13] M. D. Nardo, G. L. Calzo, M. Galea, and C. Gerada, "Design optimization of a high-speed synchronous reluctance machine," *IEEE Trans. Ind. Appl.*, vol. 54, no. 1, pp. 233–243, Jan. 2018.
[14] C. Babetto, G. Bacco, and N. Bianchi, "Synchronous reluctance machine optimization for high-speed applications," *IEEE Trans. Energy Convers.*, vol. 33, no. 3, pp. 1266–1273, Sep. 2018.
[15] Y. Hu, B. Chen, Y. Xiao, J. Shi, X. Li, and L. Li, "Rotor design and optimization of a three-phase line-start synchronous reluctance motor," *IEEE Trans. Ind. Appl.*, vol. 57, no. 2, pp. 1365–1374, Mar. 2021.
[16] N. Bianchi, M. Degano, and E. Fornasiero, "Sensitivity analysis of torque ripple reduction of synchronous reluctance and interior PM motors," *IEEE Trans. Ind. Appl.*, vol. 51, no. 1, pp. 187–195, Jan. 2015.

[17] Y. Hidaka and H. Igarashi, "Topology optimization of synchronous reluctance motors considering localized magnetic degradation caused by punching," *IEEE Trans. Magn.*, vol. 53, no. 6, pp. 1–4, Jun. 2017.
[18] N. Bianchi, S. Bolognani, D. Bon, and M. Dai Pre, "Torque harmonic compensation in a synchronous reluctance motor," *IEEE Trans. Energy Convers.*, vol. 23, no. 2, pp. 466–473, Jun. 2008.
[19] H. Mahmoud, N. Bianchi, G. Bacco, and N. Chiodetto, "Nonlinear analytical computation of the magnetic field in reluctance synchronous machines," *IEEE Trans. Ind. Appl.*, vol. 53, no. 6, pp. 5373–5382, Nov. 2017.
[20] M. Barcaro and N. Bianchi, "Air-gap flux density distortion and iron losses in anisotropic synchronous motors," *IEEE Trans. Magn.*, vol. 46, no. 1, pp. 121–126, Jan. 2010.
[21] G. Bacco and N. Bianchi, "Choice of flux-barriers position in synchronous reluctance machines," in *Proc. IEEE Energy Convers. Congr. Exposit. (ECCE)*, Jan. 2017, pp. 1872–1879.
[22] H. Mahmoud and N. Bianchi, "Eccentricity in synchronous reluctance motors—Part II: Different rotor geometry and stator windings," *IEEE Trans. Energy Convers.*, vol. 30, no. 2, pp. 754–760, Jun. 2015.
[23] N. Bianchi, S. Bolognani, D. Bon, and M. Dai Pre, "Rotor flux-barrier design for torque ripple reduction in synchronous reluctance and PM-assisted synchronous reluctance motors," *IEEE Trans. Ind. Appl.*, vol. 45, no. 3, pp. 921–928, May 2009.
[24] C. Gallardo, J. A. Tapia, M. Degano, and H. Mahmoud, "Accurate analytical model for synchronous reluctance machine with multiple flux barriers considering the slotting effect," *IEEE Trans. Magn.*, vol. 58, no. 9, pp. 1–9, Sep. 2022.
[25] C. Madariaga, W. Jara, D. Riquelme, G. Bramerdorfer, J. A. Tapia, and J. Riedemann, "Impact of tolerances on the cogging torque of tooth-coil-winding PMSMs with modular stator core by means of efficient superposition technique," *Electronics*, vol. 9, no. 10, p. 1594, Sep. 2020.
[26] S. Cai, H. Hao, M. Jin, and J. Shen, "A simplified method to analyze synchronous reluctance machine," in *Proc. IEEE Vehicle Power Propuls. Conf. (VPPC)*, Hangzhou, China, Oct. 2016, pp. 1–6.
[27] K. B. Tawfiq, M. N. Ibrahim, E. E. El-Kholy, and P. Sergeant, "Performance improvement of synchronous reluctance machines—A review research," *IEEE Trans. Magn.*, vol. 57, no. 10, pp. 1–11, Oct. 2021.
[28] G. Heins, T. Brown, and M. Thiele, "Statistical analysis of the effect of magnet placement on cogging torque in fractional pitch permanent magnet motors," *IEEE Trans. Magn.*, vol. 47, no. 8, pp. 2142–2148, Aug. 2011.

**CARLOS MADARIAGA** (Graduate Student Member, IEEE) received the B.Sc. and M.Sc. degrees in electrical engineering from Pontificia Universidad Católica de Valparaíso, Chile, in 2019 and 2020, respectively. He is currently pursuing the Ph.D. degree with the University of Concepción, Chile. He was granted a scholarship from the National Research Development Agency, in 2020, to pursue his Ph.D. studies. His current research interests include modeling, design, and optimization of high-performance electrical machines.

**CESAR GALLARDO** (Graduate Student Member, IEEE) received the B.Sc. degree in electrical engineering from the Central University "Marta Abreu" of Las Villas, Cuba, in 2016. He is currently pursuing the Ph.D. degree with the University of Concepción, Chile. He was granted a scholarship to pursue his Ph.D. studies from Agencia Nacional de Investigación y Desarrollo, in 2020. His research interests include modeling, design, and optimization of electrical machines.

**JUAN A. TAPIA** (Senior Member, IEEE) received the B.Sc. and M.Sc. degrees in electrical engineering from the University of Concepción, Concepción, Chile, in 1991 and 1997, respectively, and the Ph.D. degree from the University of Wisconsin–Madison, Madison, WI, USA, in 2002. From 2010 to 2014, he was a FiDiPro Fellow with the Academy of Finland, Lappeenranta University of Technology, Lappeenranta, Finland, where he conducted research on PM machines with LUT Energy. Currently, he is a Professor with the Department of Electrical Engineering, University of Concepción. His research interests include electrical machine design, numerical methods for electromagnetic fields, and renewable energy.

**WERNER JARA** (Member, IEEE) received the B.Sc. degree in electrical engineering from the University of Concepción, Concepción, Chile, in 2010, and the dual D.Sc. degree from the University of Concepción, and the Lappeenranta University of Technology, Lappeenranta, Finland, in 2016. He is currently a Professor with the Department of Electrical Engineering, Pontificia Universidad Católica de Valparaíso, Valparaíso, Chile. His current research interests include the field of electrical machines and drives, particularly numerical modeling and the design of electromagnetic devices.

**ANDRES ESCOBAR** was born in Valparaíso, Chile, in 1997. He received the B.Sc. and M.Sc. degrees in electrical engineering from the Pontifical Catholic University of Valparaíso, Chile, in 2021 and 2022, respectively. His research interests include modeling, control, and design of electrical machines.

**MICHELE DEGANO** (Senior Member, IEEE) received the master's degree in electrical engineering from the University of Trieste, Italy, in 2011, and the Ph.D. degree in industrial engineering from the University of Padua, Italy, in 2015. From 2014 to 2016, he was a Postdoctoral Researcher with the University of Nottingham, U.K., where he joined the Power Electronics, Machines and Control (PEMC) Research Group. In 2016, he was an Assistant Professor of advanced electrical machines with the University of Nottingham, where he was an Associate Professor, in 2020. He is currently the PEMC Director of Industrial Liaison, where he is leading research projects for the development of future hybrid electric aerospace platforms and electric transports. His current research interests include electrical machines and drives for industrial, automotive, railway, and aerospace applications ranging from small to large power.